J. Biochem. 2011;149(5):529–538 doi:10.1093/jb/mvr025

JB THE JOURNAL OF BIOCHEMISTRY

Contribution of *sams-1* and *pmt-1* to lipid homoeostasis in adult *Caenorhabditis elegans*

Received December 7, 2010; accepted December 22, 2010; published online March 9, 2011

Yingxiu Li[1], Keun Na[1], Hyoung-Joo Lee[1], Eun-Young Lee[1] and Young-Ki Paik[1,*]

[1]Department of Biochemistry and Department of Integrated OMICS for the Biomedical Science, College of Life Science and Biotechnology, World Class University Program of Graduate School, Yonsei Proteome Research Center, Yonsei University, 134 Shinchon-dong, Sudaemoon-ku, Seoul, 120-749, Korea

*Young-Ki Paik, Department of Biochemistry and Department of Integrated OMICS for the Biomedical Science, College of Life Science and Biotechnology, World Class University Program of Graduate School, Yonsei Proteome Research Center, Yonsei University, 134 Shinchon-dong, Sudaemoon-ku, Seoul, 120-749, Korea. Tel: +82-2-2123-4242, Fax: +82-2-393-6589, email: paikyk@gmail.com

Accumulation of lipids inside the cell is primarily caused by disorders of lipid metabolism. *S*-adenosylmethionine synthetase (SAMS) produces SAM, an important methyl donor in various phospholipid methyltransferase reactions catalysed by phosphoethanolamine *N*-methyltransferase (PMT-1). A gel-based, quantitative proteomic analysis of the RNA interference (RNAi)-mediated inactivation of the *pod-2* gene, which encodes acetyl-CoA carboxylase, showed a substantial down-regulation of SAMS-1. Consequently, RNAi of either *sams-1* or *pmt-1* caused a significant increase in lipid droplet size in the intestine of *Caenorhabditis elegans*. Lipid droplets exhibited increased triacylglycerol (TG) and decreased phosphatidylcholine (PC) levels, suggesting a reciprocal relationship between TG and PC regulation. These lipid-associated phenotypes were rescued by choline feeding. Among the five fat metabolism-related genes examined, two genes were highly induced by inactivation of *sams-1* or *pmt-1*: *pod-2* and stearoyl-CoA desaturase (*fat-7*). Thus, both SAMS-1 and PMT-1 were shown to contribute to the homoeostasis of TG and PC levels in *C. elegans*, which would provide an important survival strategy under harsh environmental conditions.

Keywords: *Caenorhabditis elegans*/*N*-methyltransferase/phosphatidylcholine/SAM synthetase/triglyceride.

Abbreviations: ACC, acetyl-CoA carboxylase; 2D DIGE, 2-dimensional difference gel electrophoresis; 2DE, 2-dimensional electrophoresis; CHAPS, 3-[(3-cholamidopropyl)dimethylammonio]-1-propanesulfonate; FAS, fatty acid synthase; GPAT, glycerol-3-phosphate transferase; LTQ, linear trap quadrupole; nano-LC–MS/MS, nano-liquid chromatography–tandem mass spectrometry; NGM, nematode growth medium; PC, phosphatidylcholine; PEAMT, phosphoethanolamine *N*-methyltransferase; PEMT, phosphatidylethanolamine *N*-methyltransferase; PPC, phosphocholine; SAH, *S*-adenosylhomocysteine; SAM, *S*-adenosylmethionine; SAMS, *S*-adenosylmethionine synthetase; SD, standard deviation; SREBP, sterol regulatory element-binding protein; TG, triacylglycerol.

Obesity is a pathophysiological condition in which excess body fat accumulates due to disorders in energy homoeostasis and chronic inflammation (*1*, *2*). Development of obesity involves complex interplay among multiple factors, including food intake, energy expenditure and macrophage transformation into adipocytes where triacylglycerol (TG) is stored as the main reservoir of metabolic fuel. Multiple components play a role in TG biosynthesis: acetyl-CoA carboxylase (ACC), fatty acid synthase (FAS) and glycerol-3-phosphate transferase (GPAT). Interestingly, ethanol feeding induces expression of sterol regulatory element-binding protein-1c (SREBP-1c) and its target genes, such as *pod-2* (ACC), *fasn-1* (FAS) and *gpat* (GPAT) (*3*). However, levels of these enzymes are restored to normal in the liver after supplementation with *S*-adenosylmethionine (SAM). SAM (also known as AdoMet) is an important methyl donor in various methyltransferase reactions that occur in many lipid metabolic pathways. SAM is produced by SAM synthetase (SAMS), which transfers the adenosyl portion of adenosine triphosphate to methionine. SAM-dependent methyltransferase is also involved in several methylation reactions of DNA, RNA, proteins and phospholipids (*4–6*).

Phospholipids are major components of all cell membranes and have both structural and signalling functions. Phosphatidylcholine (PC) is a major phospholipid component of the cellular membranes of eukaryotes as well as an important signal transduction molecule. In nematodes and *Plasmodium* (the causative agent of malaria in humans), PC synthesis is mediated through the SAM-dependent phosphoethanolamine *N*-methyltransferase (PEAMT) pathway, which differs sequentially from both the metabolic course of PC synthesis in mammals and the Kennedy pathway (*7–9*). Because the PEAMT genes of nematodes and *Plasmodium* lack sequence homology to eukaryotic phosphatidylethanolamine *N*-methyltransferase (PEMT) genes, including those of mammals, PEAMT is an important target of

anti-parasitic nematode agents (*7*, *10*). It was recently reported that *Caenorhabditis elegans* contains two PEAMTs, PMT-1 and PMT-2, both involved in the synthesis of phosphocholine (PPC) (*8*, *9*), which is used as a precursor for the synthesis of PC. Inactivation of the corresponding *pmt-1* or *pmt-2* genes in *C. elegans* results in P0 sterility and an F1 larval-arrest phenotype, which can be rescued by choline feeding (*8*, *9*).

It has been suggested that there is a direct reciprocal relationship between the levels of PC and TG in yeast and mammals because a decrease in PC causes an increase in TG (*11*, *12*), suggesting the existence of certain common regulatory mechanisms between the biosynthesis reactions of TG, PC and choline. To investigate this hypothesis, we asked how enzymes such as SAMS, PMT and ACC are biochemically coordinated, if at all, in lipid metabolism. To address what the potential regulatory mechanism in the formation of lipid droplets within the cell might be, we focused on the regulation of *sams-1* and *pmt-1* and explored their possible contributions to lipid homoeostasis, which is important for the survival of *C. elegans* under adverse conditions, such as starvation (*13*).

Materials and Methods

Strains

Bristol N2, a standard wild-type *C. elegans* strain, the *rrf-3(pk1426)* mutant strain and the *sams-1(ok3033)* mutant strain were obtained from the *Caenorhabditis* Genetics Center (Minneapolis, MN, USA). All strains were cultured under standard laboratory conditions using well-established procedures.

RNA interference analysis

Worms were fed *Escherichia coli* expressing RNAi constructs as described previously (*14*). The feeding constructs consisted of 554 bp *sams-1* (C49F5.1.1) and 548 bp *pmt-1* (ZK622.3 a.1). The cDNA fragments included the ligand-binding domain, and were inserted into the vector L4440 (containing two T7 RNA polymerase sites). Fragment identity was confirmed by sequencing. Constructs were transformed into HT115 *E. coli* and induced with isopropyl-β-D-thiogalactoside. For RNAi screening, feeding constructs consisted of a 439 bp *pod-2* (W09B6.1) fragment, a 524 bp *fasn-1* (F32H2.5) fragment, a 512 bp *sbp-1* (Y47D3B.7) fragment, a 524 bp *let-767* (C56G2.6.1) fragment, a 426 bp *elo-5* (F41H10.7) fragment and a 387 bp *fat-7* (F10D2.9) fragment; 136 additional RNAi-transformed *E. coli* clones from the *C. elegans* RNAi v1.1 Feeding Library (Open Biosystems, Huntsville, AL, USA) were also used.

Quantitative proteomic analysis of pod-2(RNAi) worm extracts

For two-dimensional electrophoresis (2DE), total extracts of RNAi-treated worms (100 mg) were homogenized in sample buffer (7 M urea, 2 M thiourea, 4% CHAPS [3-[(3-cholamidopropyl)-dimethylammonio]-1-propanesulfonate], 60 mM dithiothreitol, 30 mM Tris and 2 mg bromophenol blue, pH 8.5) containing protease inhibitors (Roche, Basel Switzerland) as previously described (*15*). After centrifugation, supernatants of cell lysates were treated with 50% trichloroacetic acid overnight at −20°C and centrifuged at 10,000*g* for 30 min. The pellets were washed twice with ice-cold 100% acetone, centrifuged and then re-dissolved in sample buffer. One milligram of each sample was rehydrated for 16 h at room temperature using a 24 cm Immobiline DryStrip pH 3-10NL (GE Healthcare, Uppsala, Sweden) and isoelectrically focused. The immobilized pH gradient strips were reduced and alkylated using equilibration buffer (6 M Urea, 2% SDS, 30 mM Tris, 20% glycerol, 2.5% acrylamide solution and 5 mM tributylphosphine), and finally separated by SDS-PAGE (9 ~ 16%). Gels were stained with Coomassie brilliant blue overnight, destained using ultra-pure distilled water, and then scanned with a GS710 scanning densitometer (Bio-Rad, Hemel Hempstead, UK). Analysis of the 2DE gel image was performed using Image Master Platinum 5 (GE Healthcare) (*16*). For 2D difference gel electrophoresis (2D DIGE) analysis, the cell lysates (50 mg) from the RNAi-treated worms were cross-labelled with 1 µl of 400 pmol Cy3, Cy5 and Cy2 (GE Healthcare) as described (*15*). The CyDye-labelled gels were scanned on a Typhoon 9400 scanner (GE Healthcare) at the manufacturer's recommended excitation/emission wavelengths: Cy2 (488/520 nm), Cy3 (532/580 nm) and Cy5 (633/670 nm). The gel images were analysed using DeCyder 2D analysis software v6.5.11 (GE Healthcare). Gel spot matching and statistical analysis were carried out using the biological variance analysis (BVA) module. Each gel was analysed by grouping to 'Standard', 'Control', or '*pod-2(RNAi)*' for comparisons between the different gels. A spot was accepted as statistically significant if $P < 0.05$.

Nano-liquid chromatography–tandem mass spectrometry

Nano-liquid chromatography–tandem mass spectrometry (nano-LC–MS/MS) analysis was performed on an Agilent Nano HPLC 1100 system coupled with a linear trap quadrupole (LTQ) mass spectrometer (Thermo Electron, San Jose, CA, USA) as described (*17*). Preparation of capillary columns, mobile phase solution, gradient conditions and flow rates were the same as previously described (*17*). Xcalibur 2.1 (Thermo Electron) was used for peak list generation. Mass spectra were acquired using data-dependent acquisition with a full mass scan (400–1800 m/z) followed by MS/MS scans. Each MS/MS scan acquired was an average of three microscans on the LTQ. The temperature of the ion transfer tube was controlled at 200°C, and the spray was 1.5–2.0 kV. The normalized collision energy was set at 35% for MS/MS (*17*).

Choline rescue assay

The choline concentration in the nematode growth medium (NGM) plates was adjusted to 30 mM (*9*), and the plates were seeded with *E. coli* expressing RNAi-targeted *sams-1* or *pmt-1*. Synchronized N2 worms at the L1 stage or *rrf-3(pk1426)* worms at the L3 stage were placed on control RNAi plates, *sams-1* RNAi plates or *pmt-1* RNAi plates with or without choline (30 mM) and grown at 20°C. RNAi construct-fed worms were observed under a microscope.

Lipid staining

For Sudan Black staining (*18*), *rrf-3(pk1426)* mutant worms treated with RNAi constructs, wild-type (N2) worms, and *sams-1(ok3033)* worms were washed in M9 buffer and fixed in 1% paraformaldehyde in M9 buffer. Worms were then subjected to three freeze–thaw cycles followed by dehydration in graded ethanol solutions (25, 50 and 70%). Worms were stained for 30 min in a 50% saturated solution of Sudan Black in 70% ethanol and washed once with 25% ethanol with agitation for 30 min. Oil Red O staining was performed as previously described (*19*). Briefly, the *rrf-3(pk1426)* mutant worms that had been fed RNAi constructs twice were washed and then suspended in 240 µl staining buffer composed of equal volumes of phosphate buffered saline (PBS) and 2× Modified Ruvkun's witches brew buffer (160 mM KCl, 40 mM NaCl, 14 mM Na_2EGTA, 1 mM spermidine-HCl, 0.4 mM spermine, 30 mM Na-PIPES at pH 7.4 and 0.2% β-ME) and 2% paraformaldehyde. The worms were subjected to three freeze–thaw cycles, followed by one wash in PBS, dehydration in 60% isopropanol and the addition of 60% Oil Red O staining buffer (40% water, 60% of a 0.5 g/100 ml isopropanol stock). Lipid staining was observed by microscopy.

TG and PC quantification

Synchronized L1 *rrf-3(pk1426)* mutant worms were grown on NGM agar plates covered with *E. coli* OP50, allowed to grow to the L3 stage, transferred to control RNAi plates, *sams-1* RNAi plates, or *pmt-1* RNAi plates with or without choline (30 mM) and grown at 20°C. RNAi construct-fed worms were collected from 4-day-old adult worms. RNAi construct-fed worms were frozen in liquid nitrogen and stored at −80°C until further processing. Frozen nematodes (~30 mg) were ground using a nitrogen-chilled mortar in 250 µl frozen phosphate buffer (1× PBS). Extracts were centrifuged for 7 min at 12,000*g* to clear the lysates. TG content was measured using a TG determination kit (Sigma-Aldrich, St Louis, MO, USA) as previously described (*20*), and PC content was measured using a PC assay kit (BioVision, Mountain View, CA, USA)

according to the manufacturer's instructions. Values were normalized for protein concentration as determined by the Bradford method. For each treatment condition and time point, at least two independently generated biological samples were obtained, duplicate lysates were prepared from each sample, and two measurements were taken for every preparation.

Quantitative real-time PCR

RNAi construct-fed worms were used for quantitative real-time PCR. Synchronized L1 *rrf-3(pk1426)* mutant worms were grown on NGM agar plates covered with *E. coli* OP50, allowed to grow to the L3 stage, and transferred to control RNAi plates, *sams-1* RNAi plates or *pmt-1* RNAi plates. RNAi construct-fed worms were collected from 4-day-old adult worms. Total RNA was isolated using lysis solution RA1 and a column-based illustra RNAspin mini-RNA isolation kit (GE Healthcare). RNA was treated with DNase I (Takara Bio, Otsu, Japan) as described by the manufacturer. Total RNA was reverse transcribed using the Transcriptor First Strand cDNA Synthesis kit (Roche Diagnostics, Indianapolis, IN, USA) and oligo (dT) primers (Supplementary Table SI). Quantitative real-time reverse transcription PCR (RT–PCR) was performed using an MJ Research Chromo4 Detector and the QuantiTect SYBR Green PCR kit as described by the manufacturer (Qiagen, Valencia, CA, USA) with 300 ng cDNA per sample in a total volume of 20 µl. Amplification and analysis of mRNA were performed in triplicate, and mRNA levels in the tested strains were normalized to those in the control strain and compared with one another. Serial dilutions of cDNA (300–0.3 ng) were used to construct a standard curve for quantitative real-time RT–PCR using actin as an internal control. The data presented are the mean values [±standard deviation (SD)] from triplicate determinations obtained from three independent experiments.

Green fluorescent protein reporter analysis

sams-1::gfp and *pmt-1::gfp* reporter constructs were generated by cloning *sams-1* and *pmt-1* promoters, respectively, upstream of the green fluorescent protein (GFP) gene in vector pPD95-79. The *sams-1* promoter, containing a 3318 bp sequence corresponding to a region upstream of the start codon of *sams-1* and part of the second exon (306 bp), was amplified using the following primers: *sams-1*-F (PstI), 5′-ATCTGCAGACGCAGAGGTGTAATTGAG AG-3′ (forward) and *sams-1*-R (BamHI), 5′-GGGGATCCTAATG CTGGAGTCGGTGAATCC-3′ (reverse). The *pmt-1* promoter, containing a 2568 bp sequence corresponding to a region upstream of the start of *pmt-1* and part of the first exon (25 bp), was amplified using the following primers: *pmt-1*-F (SphI), 5′-ATGCATGCCTTA AAGAAGGATGCCAGCCAAGG-3′ (forward) and *pmt*-1-R (BamHI), 5′-GGGGATCCCTGATGATTGTTGGTCGGTCG-3′ (reverse). The constructs, together with *rol-6* as a phenotypic marker, were injected into N2 worms to observe promoter-driven GFP expression patterns. To observe GFP expression in fed animals, transgenic worms were grown on OP50 bacteria and examined for GFP fluorescence from the egg to the adult stages.

Results

Proteomic analysis reveals suppression of several proteins including SAMS-1 in pod-2(RNAi) worms

From our previous studies on the *pod-2* gene, which encodes ACC, we learned that RNAi of the *pod-2* gene causes severe molting defects (Y.X. Li and Y.K. Paik, unpublished results). To examine whether any genes involved in lipid homoeostasis are influenced by *pod-2*, a rate-limiting enzyme in fatty acid biosynthesis, was inactivated. A gel-based, quantitative, proteomic analysis was carried out using control worms and *pod-2(RNAi)* worms. Figure 1A presents a typical 2DE gel image taken from one of the duplicated samples (out of two independent experiments), showing differential expression of six proteins in *pod-2(RNAi)* worms. Based on the protein spots that were differentially altered >2-fold on average, six protein spots were selected and identified by LC–MS/MS (LTQ, Table I). Representative 2D DIGE gel images (Fig. 1B) (out of three independent experiments) of the six proteins showed similar patterns of changes compared with 2DE analysis (Fig. 1A). Three classes of proteins were differentially expressed by *pod-2(RNAi)* worms: (i) three fat metabolism/transport-related proteins (protein disulfide isomerase, lipid binding protein-1 and enoyl-CoA hydratase family), (ii) two SAM cycle-related proteins [SAMS and *S*-adenosyl-L-homocysteine (SAH) hydrolase], and (iii) one protein biosynthesis-related protein (an elongation factor family member). We focused on SAMS-1, which was significantly reduced (≥2.4-fold) by *pod-2* RNAi treatment based on 2DE ($n = 2$) and 2D DIGE ($n = 3$) analyses, indicating the presence of a close relationship between *pod-2*-encoded ACC, a rate limiting enzyme in fatty acid biosynthesis, and *sams-1* function.

RNAi-mediated knock-down of sams-1 causes lipid droplet accumulation

To characterize SAMS-1 function in the context of lipid accumulation, we carried out RNAi feeding experiments and examined the phenotypes of the RNAi construct-fed worms. Interestingly, several phenotypic changes were observed in *sams–1(RNAi)* worms prepared from *rrf-3(pk1426)* worms synchronized at the L1 stage. These worms exhibited slow growth (data not shown), formation of large intestinal vacuoles (Fig. 2B) and sterile progeny. To confirm that the large intestinal vacuoles produced by RNAi-mediated knock-down of SAMS-1 were lipid droplets, we stained RNAi construct-fed worms with Sudan Black dye and observed the accumulation of enormous Sudan Black-positive lipid droplets in the intestines of *sams-1(RNAi)* worms (Fig. 2D). Furthermore, we observed large intestinal vacuoles in *sams-1(ok3033)* mutant (adult) worms (Fig. 2F); the accumulation of lipid droplets in *sams-1(ok3033)* mutants (adults) (Fig. 2H) was confirmed by Sudan Black staining. These results indicate that *sams-1* is essential for lipid homoeostasis in *C. elegans*.

Both sams-1 and pmt-1 may share the same biosynthetic pathway

Because TG synthesis is closely linked to PC synthesis (including PPC biosynthesis) and is primarily catalysed by PMT-1, we looked for similarities between the knock-down phenotype of *sams-1(RNAi)* and *pmt-1(RNAi)*. Several phenotypic changes were observed in *sams–1(RNAi)* worms prepared from *rrf-3(pk1426)* worms synchronized at the L3 stage. After 5 days when these worms reached 4-day-old adults, they showed large intestinal vacuoles (Fig. 3B), slow movement and adult fertility. Five days after RNAi treatment, we observed many large vacuoles in the intestines of *rrf-3(pk1426)* mutants that had been fed *pmt-1* RNAi beginning at the L3 stage (Fig. 3C); these worms also exhibited slow movement and adult fertility. This phenotype is quite similar to that of worms treated with *sams-1* RNAi beginning at the L3

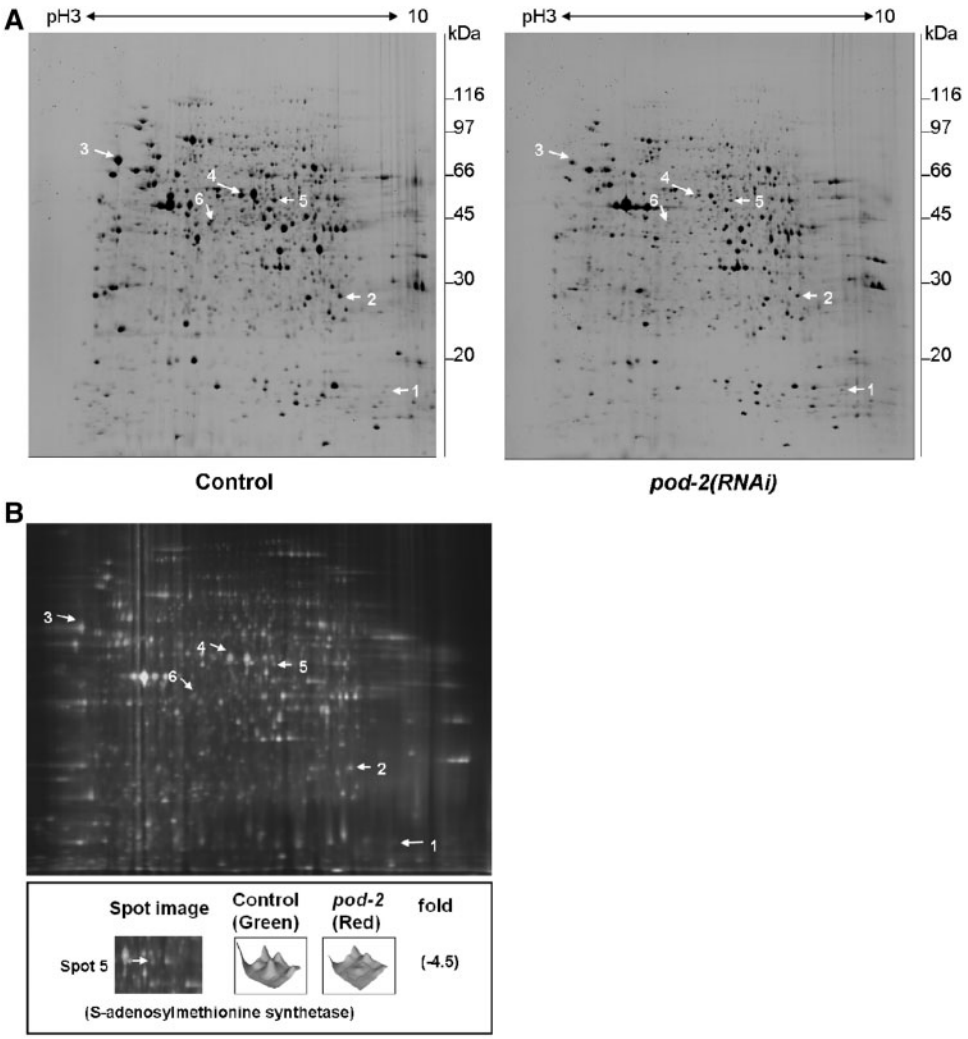

Fig. 1 2DE gel pattern of protein extracted from RNAi construct-fed worms. (A) Typical 2DE gel images are shown: control (left) and *pod-2(RNAi)* worms (right). (B) In 2D DIGE gel images, each numeral indicates a protein for which the expression level was up- or down-regulated by RNAi targeting *pod-2*. This image was taken from one of three 2D DIGE gel images.

Table I. Six differentially expressed proteins identified by 2DE, 2D DIGE and LC–MS/MS analyses.

Spot no.	Accession number	Protein name	Score	Matched peptide	Sequence coverage (%)	Average ratio (2DE)[a]	Average ratio (2D DIGE)[b]	*P*-value* (2D DIGE)
Fat metabolism/transport								
1	gi|1065518	Lipid binding protein	626	13	55	+2.6	+2.0	7.20E-05
2	gi|461983	Enoyl-CoA hydratase family member	918	17	55	−2.1	−1.4	0.0042
3	gi|13775331	Protein disulfide isomerase 2, isoform a	2,088	38	60	−3.2	−2.8	7.10E-04
SAM cycle								
4	gi|134182	*S*-adenosyl-L-homocysteine hydrolase	1,315	28	56	−2.7	−3.0	3.80E-08
5	gi|17551082	*S*-adenosylmethionine synthetase	1,054	18	43	−2.4	−4.5	6.80E-06
Protein biosynthesis								
6	gi|3123205	Elongation factor 2	583	15	16	−3.9	−1.5	0.001

[a]$n = 2$, two independent experiments.
[b]$n = 3$, three independent experiments.
*P-value and average ratio were estimated from BVA mode of 2D DIGE analyzer, DeCyder software.

stage (Fig. 3B). Sudan Black and Oil Red O staining revealed large lipid droplets in the intestines of *sams–1(RNAi)* and *pmt-1(RNAi)* worms (Fig. 3E, F, H and I). These results indicate that *sams-1* and *pmt-1* may function in the same pathway.

Choline rescues the phenotype caused by RNAi-mediated knock-down of SAMS-1 and PMT-1

Previous reports showed that PMT-1 is involved in PPC biosynthesis in *C. elegans*, and inactivation of *pmt-1* can be rescued by choline (*9*). To examine

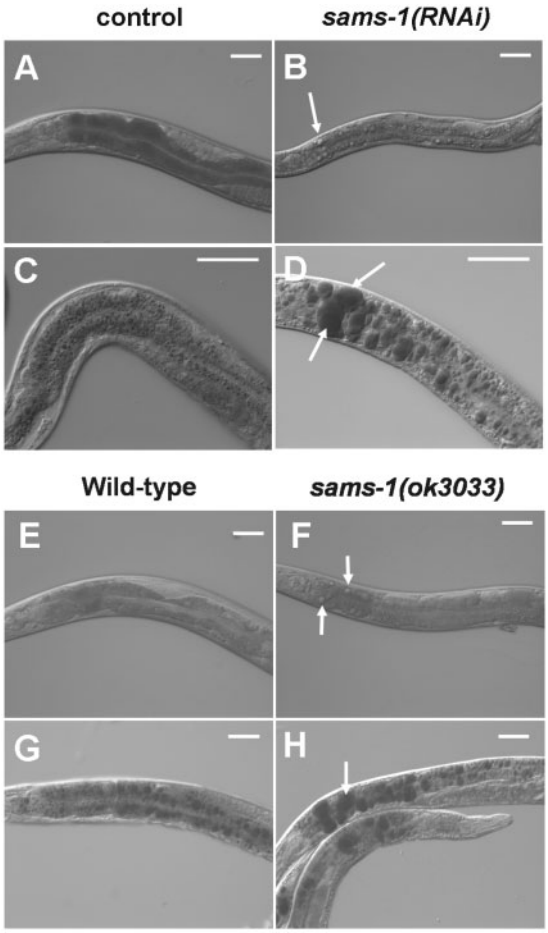

Fig. 2 Effects of RNAi-mediated knock-down of SAMS-1 in developing *C. elegans* larvae. (A and B) Worms were prepared by feeding RNAi-expressing *E. coli* to larvae. (A) Control worm that received plasmid L4440 only. (B) An *rrf-3(pk1426)* worm fed *sams-1* RNAi-expressing *E. coli* beginning at the L1 stage. After 5 days, *sams-1(RNAi)* worms showed slow growth and formed large intestinal vacuoles; their progeny were also sterile. Arrow indicates a large vacuole. Scale bar, 50 μm. (C and D) Changes in lipid content in an RNAi worm as detected by Sudan Black staining. *rrf-3 (pk1426)* L1 larvae were fed bacteria expressing RNAi constructs targeting the indicated genes. (C) Control worm that received plasmid L4440 only. (D) Worm fed *sams-1* RNAi after 5 days, showing intestinal lipid droplet accumulation. Arrows indicate large lipid droplets. Scale bar, 50 μm. (E) Wild-type (N2) worm. (F) *sams-1(ok3033)* mutant, showing intestinal vacuoles. Arrows indicate large vacuoles. Scale bar, 50 μm. (G and H) Changes in lipid content in wild-type and *sams-1(ok3033)* mutant worms as detected by Sudan Black staining. (G) Wild-type (N2) worm. (H) *sams-1 (ok3033)* mutant worm, showing intestinal lipid droplet accumulation. Arrow indicates a large lipid droplet. Scale bar, 50 μm.

whether *sams-1* is involved in the PPC biosynthetic pathway in which *pmt-1* is known to participate, we carried out choline rescue experiments using *sams-1(RNAi)* worms; *pmt-1(RNAi)* worms were used as a positive control. We also used N2 wild-type worms as a control because they have been used routinely in many laboratories. To confirm the sterile phenotype of *sams-1(RNAi)* and *pmt-1(RNAi)* worms in the wild-type background, L1-stage synchronized N2 worms were treated with control, *sams-1* RNAi and *pmt-1* RNAi, respectively. After 5 days, eggs were present in the control worm, but no eggs were found in either the *sams-1(RNAi)* or *pmt-1(RNAi)* worms (Supplementary Fig. S1). We then conducted the choline rescue assay such that L1-stage synchronized N2 worms were placed on RNAi plates with or without 30 mM choline and grown for 5 days. As expected, control worms showed normal growth (Fig. 4A and B), whereas *sams-1(RNAi)* worms grown in the absence of choline (Fig. 4C) exhibited abnormal phenotypes, such as slow movement and formation of sterile progeny. In contrast, the presence of choline rescued the sterile progeny phenotype of *sams-1(RNAi)* worms and restored normal growth (Fig. 4D). In addition, *pmt-1(RNAi)* worms were rescued by choline, which restored both normal growth and adult fertility (Fig. 4E and F). After synchronization at the L1 stage, we grew *rrf-3(pk1426)* mutants to the L3 stage on NGM plates and then transferred them to RNAi plates with or without 30 mM choline. The large vacuoles present in the intestines of *sams-1(RNAi)* worms were nearly eliminated by choline feeding (Fig. 4I and J). This phenomenon was also observed in *pmt-1(RNAi)* worms (Fig. 4K and L), suggesting that SAMS-1 functions in the same PPC biosynthetic pathway as PMT-1.

To examine the spatial and temporal expression patterns of these genes, we constructed transgenic *sams-1::gfp* worms and *pmt-1::gfp* worms in which GFP expression is driven by the *sams-1* and *pmt-1* promoters, respectively. The transcriptional activity *sams-1::gfp* was observed primarily in the body wall muscle and nerve cord throughout all developmental stages (Fig. 5B), whereas *pmt-1::gfp* transcriptional activity was observed primarily in the hypodermis during embryogenesis and in all four larval stages (Fig. 5D). *pmt-1::gfp* was also expressed in seam cells, but only in the adult stage (Fig. 5F), indicating the developmental expression of PMT-1 in seam cells.

Down-regulation of sams-1 or pmt-1 leads to TG accumulation and a reduction in PC content

In yeast, a decrease in *de novo* PC synthesis and an increase in TG levels can be induced by the down-regulation of SAH hydrolase, which acts as an inhibitor of SAM-dependent methyltransferase (*12*), a homologue of PMT-1 in *C. elegans*. Therefore, we hypothesized that a decrease in the PPC biosynthesis-related genes *sams-1* and *pmt-1* would alter the homoeostatic balance between PC synthesis and TG storage in *C. elegans* and would consequently increase the TG content of lipid droplets (Fig. 6). To determine the involvement of *sams-1* and *pmt-1* in TG storage, we measured total TG levels in both *sams-1(RNAi)* and *pmt-1(RNAi)* worms and then performed choline rescue assays. Total TG levels in *sams-1*(*RNAi*) and *pmt-1(RNAi)* worms increased by 155 ± 11% (in three experiments) and 138 ± 9% (in three experiments), respectively, compared with levels in control worms (Fig. 6A). These results demonstrate that both *sams-1* and *pmt-1* are involved in TG metabolism. To confirm that *sams-1* is involved in the PC synthetic pathway in which *pmt-1* is known to participate, we determined PC levels in *sams-1(RNAi)* and

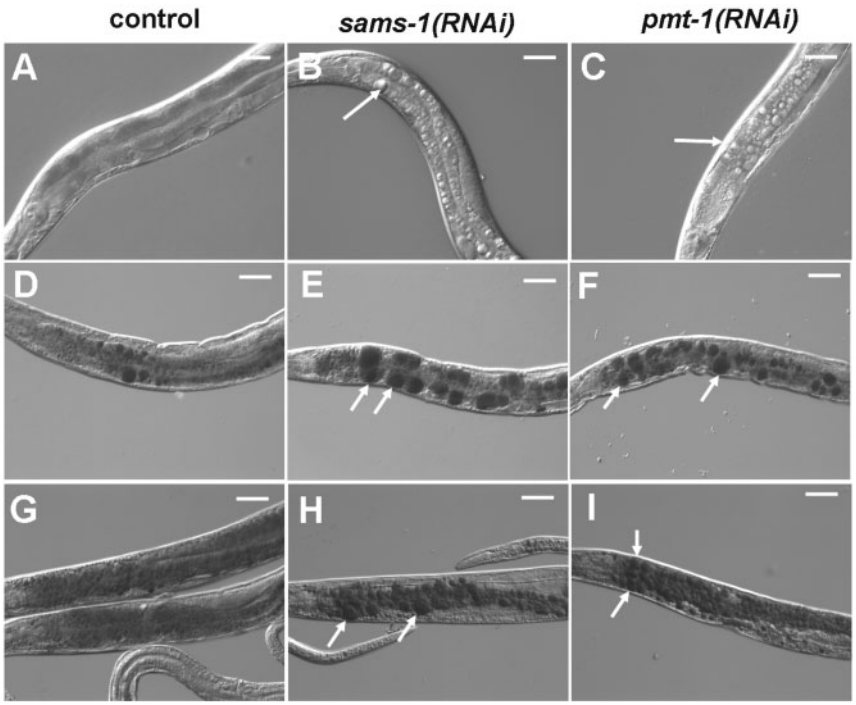

Fig. 3 Phenotypes of *sams-1(RNAi)* and *pmt-1(RNAi)* worms. (A–I) *rrf-3(pk1426)* L3 larvae were fed bacteria expressing RNAi targeting the indicated gene or plasmid L4440 only (control). (A) Control worm. (B) *sams-1(RNAi)* worm. (C) *pmt-1(RNAi)* worm. *sams-1(RNAi)* and *pmt-1(RNAi)* worms showed similar phenotypes, which included large vacuoles in the intestines after 5 days. Arrows indicate large vacuoles. Scale bar, 50 μm. (D–F) Changes in lipid content in RNAi construct-fed worms as detected by Sudan Black staining. (D) Control worm. (E) *sams-1(RNAi)* worm. (F) *pmt-1(RNAi)* worm. *sams-1(RNAi)* and *pmt-1(RNAi)* worms showed similar lipid droplet accumulation in the intestines after 5 days. Arrows indicate large lipid droplets. Scale bar, 50 μm. (G–I) Changes in lipid content in RNAi construct-fed worms as detected by Oil Red O staining. (G) Control worm. (H) *sams-1(RNAi)* worm. (I) *pmt-1(RNAi)* worm. *sams-1(RNAi)* and *pmt-1(RNAi)* worms showed similar lipid droplet accumulation in the intestines after 5 days. Arrows indicate large lipid droplets. Scale bar, 50 μm.

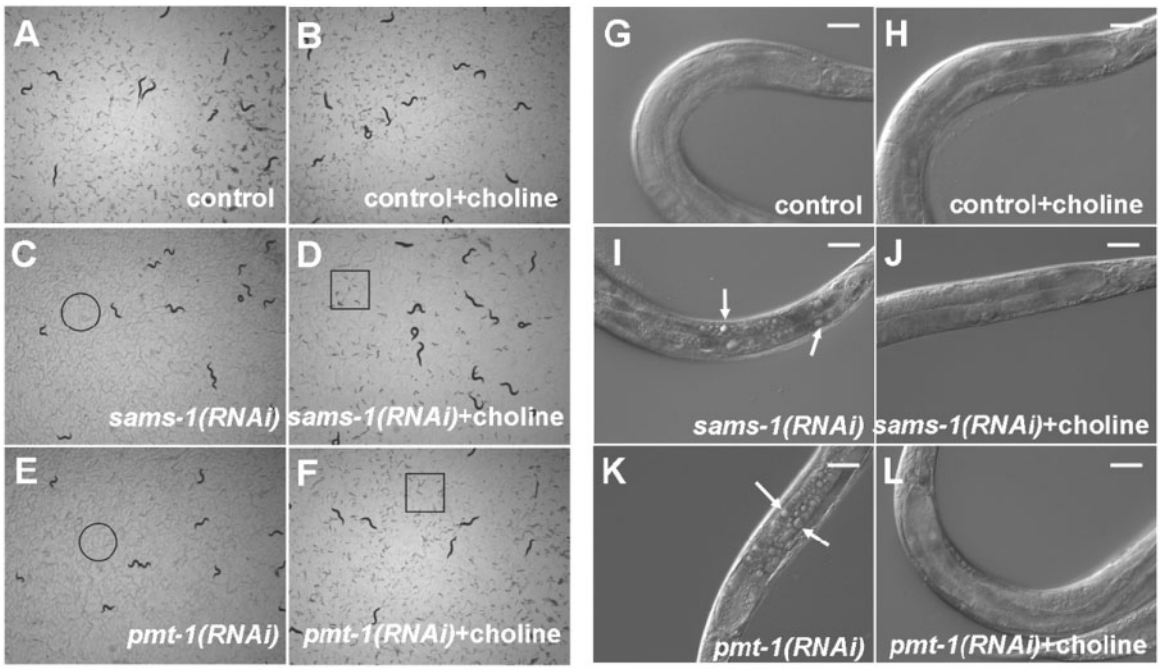

Fig. 4 Rescue of the *sams-1(RNAi)* and *pmt-1(RNAi)* phenotypes by supplementing with choline. (A–F) N2 worms synchronized at L1 were placed on an RNAi plate with or without 30 mM choline containing bacteria expressing RNAi targeting the indicated gene or plasmid L4440 only (control). (A) Control worms; (B) control worms plus choline; (C) *sams-1(RNAi)* worms, showing sterile progeny (no F1 progeny; circle); (D) *sams-1(RNAi)* worms plus choline, showing normal growth and fertile adults with many F1 progeny (box); (E) *pmt-1(RNAi)* worms, showing abnormal growth and reproduction; and (F) *pmt-1(RNAi)* worms plus choline, showing normal growth and reproduction. (G–L) Synchronized L1-stage *rrf-3(pk1426)* mutants were grown to the L3 stage on an NGM plate and then transferred to an RNAi plate with or without 30 mM choline containing bacteria expressing RNAi targeting the indicated gene or plasmid L4440 only (control). (G) Control worm; (H) control worm plus choline; (I) *sams-1(RNAi)* worm, showing large vacuoles in the intestine (arrows); (J) *sams-1(RNAi)* worm plus choline, showing normal intestine without large vacuoles; (K) *pmt–1(RNAi)* worm, showing the large-vacuole (intestine) phenotype (arrows); and (L) *pmt–1(RNAi)* worm plus choline, showing normal intestine without large vacuoles. Scale bar, 50 μm.

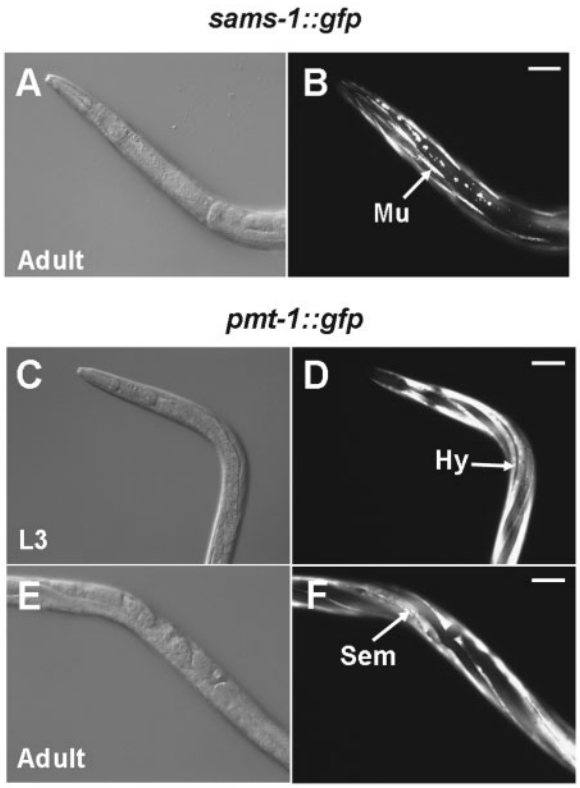

Fig. 5 Transgenic worms expressing *sams-1::gfp* and *pmt-1::gfp* as a readout for *sams-1* and *pmt-1* expression patterns. Expression of GFP in transgenic worms was imaged by bright field and GFP fluorescence microscopy. Scale bar, 50 μm. (A and B) Transgenic worms expressing *sams-1::gfp* constructs in which GFP expression is driven by the *sams-1* promoter. Expression of *sams-1::gfp* in the body muscle (Mu) [arrow in (B)]. (A) Nomarski image of the adult head shown in (B). Expression of *sams-1::gfp* in body wall muscle and nerve cord. (C–F) Transgenic worms expressing *pmt-1::gfp* constructs in which GFP expression is driven by the *pmt-1* promoter. (C and D) Expression of *pmt-1::gfp* in the hypodermis (Hy) [arrow in (D)] but not in seam cells. (C) Nomarski image of the L3 larva shown in (D). (E, F) Expression of *pmt-1::gfp* in hypodermis-containing seam cell (Sem) [arrow in (F)]. (E) Nomarski image of the adult shown in (F).

pmt-1(RNAi) worms and in choline-rescued RNAi construct-fed worms. Total levels of PC in *sams-1(RNAi)* and *pmt-1(RNAi)* worms decreased by 73 ± 6.6% (in three experiments) and 35 ± 0.3% (in three experiments), respectively, compared with levels in control worms (Fig. 6B). Collectively, these results show that down-regulation of *sams-1* or *pmt-1* leads to TG accumulation and a decrease in PC, confirming that *sams-1*, like *pmt-1*, is involved in PC synthesis. These results further illustrate an apparent homoeostasis between TG and PC in *C. elegans*.

Both sams-1 and pmt-1 are coupled to the expression of lipid regulatory genes

To both examine how *sams-1* regulates lipid storage and identify genes that are involved in decreasing the large vacuoles/lipid granules in *sams-1(RNAi)* worms (Supplementary Table SII), we performed RNAi screening by individually inactivating 142 fatty acid metabolism-related genes. We observed similar RNAi phenotypes with either *sams-1* RNAi alone or in the presence of L4440. These worms possessed large vacuoles in their intestines. At the same time, we observed whether the phenotypes of large vacuoles would disappear when *sams-1* RNAi was performed in the presence of each gene. We found that inactivation of any of five potential regulatory genes—*pod-2*, *fasn-1*, *fat-7*, *sbp-1* or *let-767*—not only eliminated the large vacuoles in *sams-1(RNAi)* worms (Supplementary Fig. S1) but also reduced the dark intestinal coloration in each worm receiving RNAi treatment of one of the five genes, suggesting that the stored lipid might have been used (Supplementary Fig. S2). The purpose of RNAi screening was to identify those genes that might influence lipid accumulation, while quantitative real-time RT–PCR was performed to find the relationship between them. To further explore the regulation of these five genes by *sams-1,* we measured their mRNA levels in *sams-1(RNAi)* worms. We found that the mRNA levels of *pod-2* and *fat-7* were increased significantly in *sams–1(RNAi)* worms (161 ± 24% and 619 ± 36%, respectively, in three experiments) compared to controls (Fig. 6C). Both *pod-2* and *fat-7* were increased ~3.2- and 16.4-fold, respectively, in *pmt-1(RNAi)* worms, whereas *fasn-1* levels remained unchanged. Both *sbp-1* and *let-767* were slightly increased only in *pmt-1(RNAi)* worms (Fig. 6C). These results suggest that there might be a dynamic relationship between fatty acid biosynthesis and desaturation in the context of *sams-1* and *pmt-1* inactivation.

Discussion

This is the first report showing that *sams-1* and *pmt-1* genes are actively involved in lipid storage in *C. elegans* and that the coordinated expression of both genes contributes to the homoeostasis between PC and TG biosynthesis (Fig. 6D). Our proteomic data suggest that a feedback loop exists between *pod-2* and *sams-1*, i.e., *pod-2* RNAi causes a parallel decrease in *sams-1*, but the knock-down of *sams-1* results in the induction of *pod-2*, leading to TG accumulation. PMT-1 has been previously shown to be involved in PPC biosynthesis in *C. elegans*; a PMT-1 defect is rescued by choline (*9*). Our data show that the phenotype (e.g., lipid accumulation) of *sams-1(RNAi)* worms is similar to that of *pmt-1(RNAi)* worms and can be rescued by choline, suggesting that *sams-1* is actively involved in PPC biosynthesis, which occurs via a PEAMT route. This mechanism involves a completely different pathway from the PEMT pathway of host organisms of parasitic nematodes (*8*, *9*). The biochemical basis for the coordinated expression of *sams-1* and *pmt-1* may stem from the fact that PMT-1 uses SAM for a substrate and is inhibited by SAH (*9*). Since SAM is soluble (in the case of mammals) and is known to be involved in most cellular methyltransferse reactions, it has been speculated that SAM could be produced in muscle as well as nerve tissue and transported to other tissues (e.g., hypodermis) under specific conditions, such as good nutrition, in *C. elegans*. Grabitzki *et al.* (*21*) identified 69 PPC-modified proteins involved in

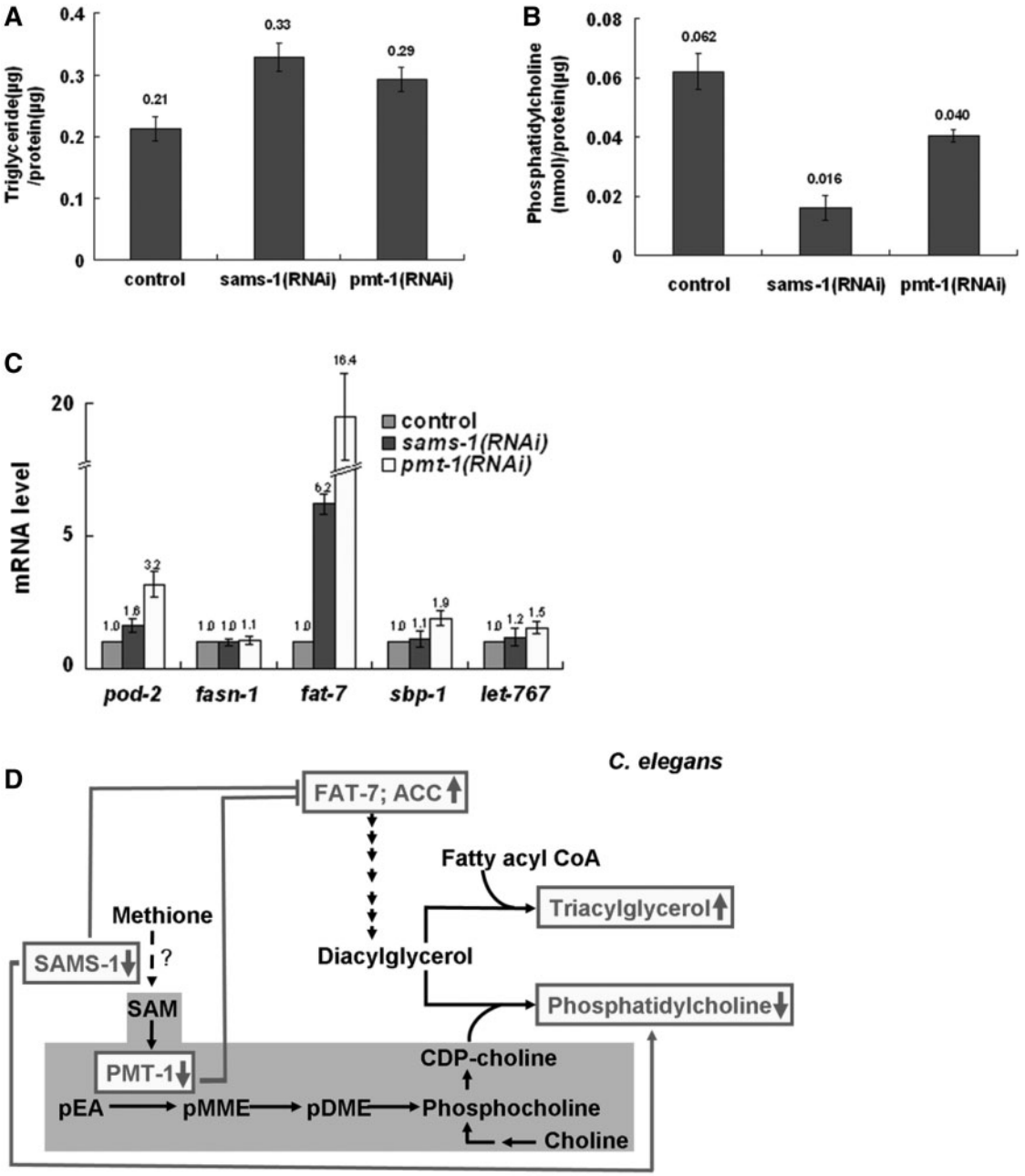

Fig. 6 A cooperative role for *sams-1* and *pmt-1* in TG and PC biosynthesis. Comparison of the amounts of TG (A) and PC (B) in RNAi construct-fed worms. Evaluation of mRNA levels by quantitative real-time PCR. Worms were fed bacteria expressing empty vector (control) or *sams-1* RNAi or *pmt-1* RNAi (C) beginning at the L3 stage. Data are the average (±SD) of three experiments. (D) A working model of the cooperative role for *sams-1* and *pmt-1* in TG and PC biosynthesis.

metabolism, structure, protein degradation or signalling; one of these proteins is peroxisomal 3-ketoacyl-CoA thiolase (DAF-22, Y57A10C.6). The *daf-22(ok693)* mutant has defects in peroxisomal β-oxidation and causes the accumulation of lipid droplets in the intestine (*22*, *23*). Decreased levels of PPC may affect the peroxisomal β-oxidation pathway through DAF-22. Although the expression levels of *sams-1* and *pmt-1* cannot be detected in the intestine, we conjecture that *sams-1* and *pmt-1* may function non-cell autonomously in the intestinal lipid metabolism processes of *C. elegans*. With respect to possible transporters for SAM and pMME, it is not clear yet in *C. elegans*. Perhaps, they would be converted to PPC and then transported to other cells, which remains to be verified.

In alcoholic steatohepatitis caused by excessive alcohol intake, SAM levels are reduced, the PEMT pathway is suppressed and SREBP-1 c levels are increased in association with TG accumulation in the liver (*3*). These findings are consistent with our observation that SAM biosynthesis is directly involved in TG biosynthesis in *C. elegans*, suggesting SAMS-1 is an important regulatory enzyme. For example, Ashrafi *et al.* (*24*)

previously reported that lipid accumulation was decreased when the expression of *sams-2*, *sams-3*, *sams-4* and *sams-5* was inactivated by RNAi knock-down. These results show that SAMS-1 plays an important role in lipid metabolism in *C. elegans*.

Consumption of CDP-choline causes an accumulation of diacylglycerol molecules because of TG formation (*11*). SAH hydrolase converts SAM to SAH, an inhibitor of methyltransferases in humans (*25*). The accumulation of SAH in yeast has been shown to lead to a decrease in the conversion of PE to PC, resulting in TG accumulation (*12*). These data are consistent with our demonstration that TG content increases when the concentration of PC decreases (Fig. 6D). Our results show that PC levels in *sams-1(RNAi)* and *pmt-1(RNAi)* worms tend towards normal levels following choline rescue (data not shown). Therefore, although the pathway of PC biosynthesis in *C. elegans* differs from those in yeast and mammals, the balance between PC and TG remains identical in *C. elegans*.

LET-767 is the 3-ketoacyl CoA reductase in *C. elegans*, and *let-767(RNAi)* worms have been shown to exhibit a decrease in the total amount of fatty acids stored in the form of TG (*26*). Using RNAi screening, we found that the inactivation of *pod-2*, *fasn-1*, *fat-7*, *sbp-1*, or *let-767* caused a decrease in lipid storage in *sams-1(RNAi)* worms (Supplementary Fig. S2). Furthermore, mRNA levels of *pod-2* and *fat-7* increased significantly in both *sams-1(RNAi)* and *pmt-1(RNAi)* worms. The higher magnitude of the increase in *pod-2* and *fat-7* in *pmt-1(RNAi)* worms compared to *sams-1(RNAi)* worms may be because *pmt-1* is more likely positioned at the rate-limiting step, which directly influences ACC and stearyl-CoA desaturase activities (Fig. 6D). From these results, we conclude that *pod-2*, *fasn-1*, *fat-7*, *sbp-1* and *let-767* are essential for TG biosynthesis in *C. elegans* and that the TG accumulation caused by RNAi-mediated knock-down of SAMS-1 or PMT-1 results from the activation of *pod-2* and *fat-7* (Fig. 6D). This finding is consistent with the notion that increases in TG content accompany a decrease in phospholipids in *daf-2* mutants (*24*).

In conclusion, the coordinated expression of *sams-1* and *pmt-1* not only contributes to the homoeostasis of lipid distribution but also establishes a reciprocal relationship between the biosynthesis of both PC and TG in *C. elegans*. Down-regulation of either *sams-1* or *pmt-1* leads to TG accumulation and a decrease in PC, demonstrating a new role for *sams-1* in PC biosynthesis. Our results also imply that the TG accumulation caused by RNAi-mediated knock-down of SAMS-1 or PMT-1 might be due to the activation of either *pod-2* or *fat-7*. Because PMT-1 has been suggested to be a target of anti-parasitic nematode agents (*9*), SAMS-1 may also be a viable target of anti-parasitic drug development efforts but remains to be validated.

Supplementary Data

Supplementary Data are available at *JB* Online.

Acknowledgements

We thank the *Caenorhabditis* Genetics Center for providing the *rrf-3(pk1426)* mutants.

Funding

Korean Health 21 R&D Project, Ministry of Health and Welfare, Republic of Korea (A030003 to Y.K.P.); Ministry of Education, Science and Technology (National Research Foundation of Korea, World Class University program, R31-2008-000-10086-0).

Conflict of interest

None declared.

References

1. Badman, M.K. and Flier, J.S. (2007) The adipocyte as an active participant in energy balance and metabolism. *Gastroenterology* **132**, 2103–2115
2. Watts, J.L. (2009) Fat synthesis and adiposity regulation in *Caenorhabditis elegans*. *Trends Endocrinol. Metab.* **20**, 58–65
3. Esfandiari, F., You, M., Villanueva, J.A., Wong, D.H., French, S.W., and Halsted, C.H. (2007) S-adenosylmethionine attenuates hepatic lipid synthesis in micropigs fed ethanol with a folate-deficient diet. *Alcohol. Clin. Exp. Res.* **31**, 1231–1239
4. Chiang, P.K., Gordon, R.K., Tal, J., Zeng, G.C., Doctor, B.P., Pardhasaradhi, K., and McCann, P.P. (1996) S-adenosylmethionine and methylation. *FASEB J.* **10**, 471–480
5. Tehlivets, O., Hasslacher, M., and Kohlwein, S.D. (2004) S-adenosyl-L-homocysteine hydrolase in yeast: key enzyme of methylation metabolism and coordinated regulation with phospholipid synthesis. *FEBS Lett.* **577**, 501–506
6. Yi, P., Melnyk, S., Pogribna, M., Pogribny, I.P., Hine, R.J., and James, S.J. (2000) Increase in plasma homocysteine associated with parallel increases in plasma S-adenosylhomocysteine and lymphocyte DNA hypomethylation. *J. Biol. Chem.* **275**, 29318–29323
7. Pessi, G., Kociubinski, G., and Mamoun, C.B. (2004) A pathway for phosphatidylcholine biosynthesis in *Plasmodium falciparum* involving phosphoethanolamine methylation. *Proc. Natl. Acad. Sci. USA* **101**, 6206–6211
8. Palavalli, L.H., Brendza, K.M., Haakenson, W., Cahoon, R.E., McLaird, M., Hicks, L.M., McCarter, J.P., Williams, D.J., Hresko, M.C., and Jez, J.M. (2006) Defining the role of phosphomethylethanolamine *N*-methyltransferase from *Caenorhabditis elegans* in phosphocholine biosynthesis by biochemical and kinetic analysis. *Biochemistry* **45**, 6056–6065
9. Brendza, K.M., Haakenson, W., Cahoon, R.E., Hicks, L.M., Palavalli, L.H., Chiapelli, B.J., McLaird, M., McCarter, J.P., Williams, D.J., Hresko, M.C., and Jez, J.M. (2007) Phosphoethanolamine N-methyltransferase (PMT-1) catalyses the first reaction of a new pathway for phosphocholine biosynthesis in *Caenorhabditis elegans*. *Biochem. J.* **404**, 439–448
10. Nirmalan, N., Sims, P.F., and Hyde, J.E. (2004) Quantitative proteomics of the human malaria parasite *Plasmodium falciparum* and its application to studies of development and inhibition. *Mol. Microbiol.* **52**, 1187–1199
11. Caviglia, J.M., De Gómez Dumm, I.N., Coleman, R.A., and Igal, R.A. (2004) Phosphatidylcholine deficiency upregulates enzymes of triacylglycerol metabolism in CHO cells. *J. Lipid Res.* **45**, 1500–1509

12. Malanovic, N., Streith, I., Wolinski, H., Rechberger, G., Kohlwein, S.D., and Tehlivets, O. (2008) S-adenosyl-L-homocysteine hydrolase, key enzyme of methylation metabolism, regulates phosphatidylcholine synthesis and triacylglycerol the homeostasis in yeast: implications for homocysteine as a risk factor of atherosclerosis. *J. Biol. Chem.* **283**, 23989–23999
13. Jeong, P.Y., Kwon, M.S., Joo, H.J., and Paik, Y.K. (2009) Molecular time-course and the metabolic basis of entry into dauer in *Caenorhabditis elegans*. *PLoS ONE* **4**, e4162
14. Timmons, L. and Fire, A. (1998) Specific Interference by ingested dsRNA. *Nature* **395**, 854
15. Jeong, P.Y., Na, K., Jeong, M.J., Chitwood, D., Shim, Y.H., and Paik, Y.K. (2009) Proteomic analysis of *Caenorhabditis elegans*. *Methods Mol. Biol.* **519**, 145–169
16. Choi, B.K., Shin, Y.K., Lee, E.Y., Jeong, P.Y., Shim, Y.H., Chitwood, D.J., and Paik, Y.K. (2009) Proteomic analysis of the sterol-mediated signaling pathway in *Caenorhabditis elegans*. *Methods Mol. Biol.* **462**, 181–195
17. Lee, H.J., Kang, M.J., Lee, E.Y., Cho, S.Y., Kim, H., and Paik, Y.K. (2008) Application of a peptide-based PF2D platform for quantitative proteomics in disease biomarker discovery. *Proteomics* **8**, 3371–3381
18. McKay, R.M., McKay, J.P., Avery, L., and Graff, J.M. (2003) *C. elegans*: a model for exploring the genetics of fat storage. *Dev. Cell* **4**, 131–142
19. Soukas, A.A., Kane, E.A., Carr, C.E., Melo, J.A., and Ruvkun, G. (2009) Rictor/TORC2 regulates fat metabolism, feeding, growth and life span in *Caenorhabditis elegans*. *Genes Dev.* **23**, 496–511
20. Ristow, M., Pfister, M.F., Yee, A.J., Schubert, M., Michael, L., Zhang, C.Y., Ueki, K., Michael, M.D., Lowell, B.B., and Kahn, C.R. (2000) Frataxin activates mitochondrial energy conversion and oxidative phosphorylation. *Proc. Natl. Acad. Sci. USA* **97**, 12239–12243
21. Grabitzki, J., Ahrend, M., Schachter, H., Geyer, R., and Lochnit, G. (2008) The PCome of *Caenorhabditis elegans* as a prototypic model system for parasitic nematodes: identification of phosphorylcholine-substituted proteins. *Mol. Biochem. Parasitol.* **161**, 101–111
22. Joo, H.J., Yim, Y.H., Jeong, P.Y., Jin, Y.X., Lee, J.E., Kim, H., Jeong, S.K., Chitwood, D.J., and Paik, Y.K. (2009) *Caenorhabditis elegans* utilizes dauer pheromone biosynthesis to dispose of toxic peroxisomal fatty acids for cellular homoeostasis. *Biochem. J.* **422**, 61–71
23. Zhang, S.O., Box, A.C., Xu, N., Le Men, J., Yu, J., Guo, F., Trimble, R., and Mak, H.Y. (2010) Genetic and dietary regulation of lipid droplet expansion in *Caenorhabditis elegans*. *Proc. Natl. Acad. Sci. USA* **107**, 4640–4645
24. Ashrafi, K., Chang, F.Y., Watts, J.L., Fraser, A.G., Kamath, R.S., Ahringer, J., and Ruvkun, G. (2003) Genome-wide RNAi analysis of *Caenorhabditis elegans* fat regulatory genes. *Nature* **421**, 268–272
25. Altintas, E. and Sezgin, O. (2004) S-adenosylhomocysteine hydrolase, S-adenosylmethionine, S-adenosylhomocysteine: correlations with ribavirin induced anemia. *Med. Hypotheses* **63**, 834–837
26. Entchev, E.V., Schwudke, D., Zagoriy, V., Matyash, V., Bogdanova, A., Habermann, B., Zhu, L., Shevchenko, A., and Kurzchalia, T.V. (2008) LET-767 is required for the production of branched chain and long chain fatty acids in *Caenorhabditis elegans*. *J. Biol. Chem.* **283**, 17550–17560